$(Ca_{0.37}Sr_{0.63})TiO_3$ perovskite—an example of an unusual class of tilted perovskites

2008 J. Phys.: Condens. Matter 20 135202

(http://iopscience.iop.org/0953-8984/20/13/135202)

J. Phys.: Condens. Matter **20** (2008) 135202 (11pp) doi:10.1088/0953-8984/20/13/135202

$(Ca_{0.37}Sr_{0.63})TiO_3$ perovskite—an example of an unusual class of tilted perovskites

C J Howard[1,4], R L Withers[2], K S Knight[3] and Z Zhang[1]

[1] Australian Nuclear Science and Technology Organisation, Private Mail Bag 1, Menai, NSW 2234, Australia
[2] Research School of Chemistry, Australian National University, Canberra, A.C.T. 0200, Australia
[3] ISIS Facility, Rutherford Appleton Laboratory, Chilton, Didcot, Oxfordshire, OX11 0QX, UK

Received 30 November 2007, in final form 4 February 2008
Published 7 March 2008
Online at stacks.iop.org/JPhysCM/20/135202

Abstract

The structure of $Ca_{0.37}Sr_{0.63}TiO_3$ perovskite has been carefully investigated using electron and neutron diffraction. Electron diffraction supports the supercell and *Pbcm* space group previously proposed, while high resolution neutron powder diffraction data provide the basis for a new structure refinement. The distortions of the resultant structure relative to the ideal parent perovskite structure type have been decomposed into normal modes. It is found that the primary modes of distortion are octahedral tilting modes associated with the R point ($\mathbf{k} = [1/2, 1/2, 1/2]^*$) and the $\xi = 1/4$ point on the T line of symmetry ($\mathbf{k} = [1/2, 1/2, \xi]^*$). There is a smaller secondary, probably induced, mode of distortion involving antiferroelectric displacements of the Ti cations associated with the $\xi = 1/4$ point on the Δ line of symmetry ($\mathbf{k} = [0, 0, \xi]^*$). This compound provides one of the very few currently known examples of a tilted perovskite structure that shows tilting modes associated with the ubiquitous $\mathbf{k} = \langle 1/2, 1/2, \xi \rangle^*$ modulation wavevectors for a value of ξ different from 0 and 1/2.

(Some figures in this article are in colour only in the electronic version)

1. Introduction

The $CaTiO_3$–$SrTiO_3$ system has attracted a great deal of attention over many years as a result of both the general importance of perovskites to the earth sciences of the lower mantle as well as to a proposal that $CaTiO_3$ could be used as containment for the radioactive Sr ions from radioactive waste (Redfern 1996, Ringwood *et al* 1988). Recently, on the basis of the large amount of available data, Carpenter *et al* (2006) have presented a temperature–composition phase diagram for the $CaTiO_3$–$SrTiO_3$ system. One of the most interesting aspects in that paper is the occurrence of a structure with unit cell of dimensions $\sqrt{2}a_p \times \sqrt{2}a_p \times 4a_p$ (with respect to the cell edge, a_p, of the underlying parent perovskite sub-structure) and a space group symmetry *Pbcm*. This structure was first noted by Ranjan *et al* (2000), then refined from neutron data by Mishra *et al* (2002) and from x-ray data by Mishra *et al* (2006). The structure is found in the $Ca_{1-x}Sr_xTiO_3$ system for compositions $0.59 \leqslant x \leqslant 0.84$ at low temperature and for $0.59 \leqslant x \leqslant 0.65$ at room temperature (Carpenter *et al* 2006). This *Pbcm* structure, specifically at the composition $Ca_{0.37}Sr_{0.63}TiO_3$ (CST63), provides the subject matter for this paper.

We report first on experimental investigations of the structure of $Ca_{0.37}Sr_{0.63}TiO_3$ by electron diffraction, and then by neutron powder diffraction. The electron diffraction evidence confirms the unit cell (including the unusual quadrupling relative to the parent perovskite cell edge), as well as *Pbcm* space group symmetry. The structures at 4.2 and 293 K have then been refined from high quality, high resolution neutron powder diffraction data. We report coordinates that we believe are rather more reliable than those published previously.

In the following section we use group theoretical techniques to enumerate and describe the various distortions,

[4] Present address: School of Engineering, The University of Newcastle, Callaghan, NSW 2308, Australia.

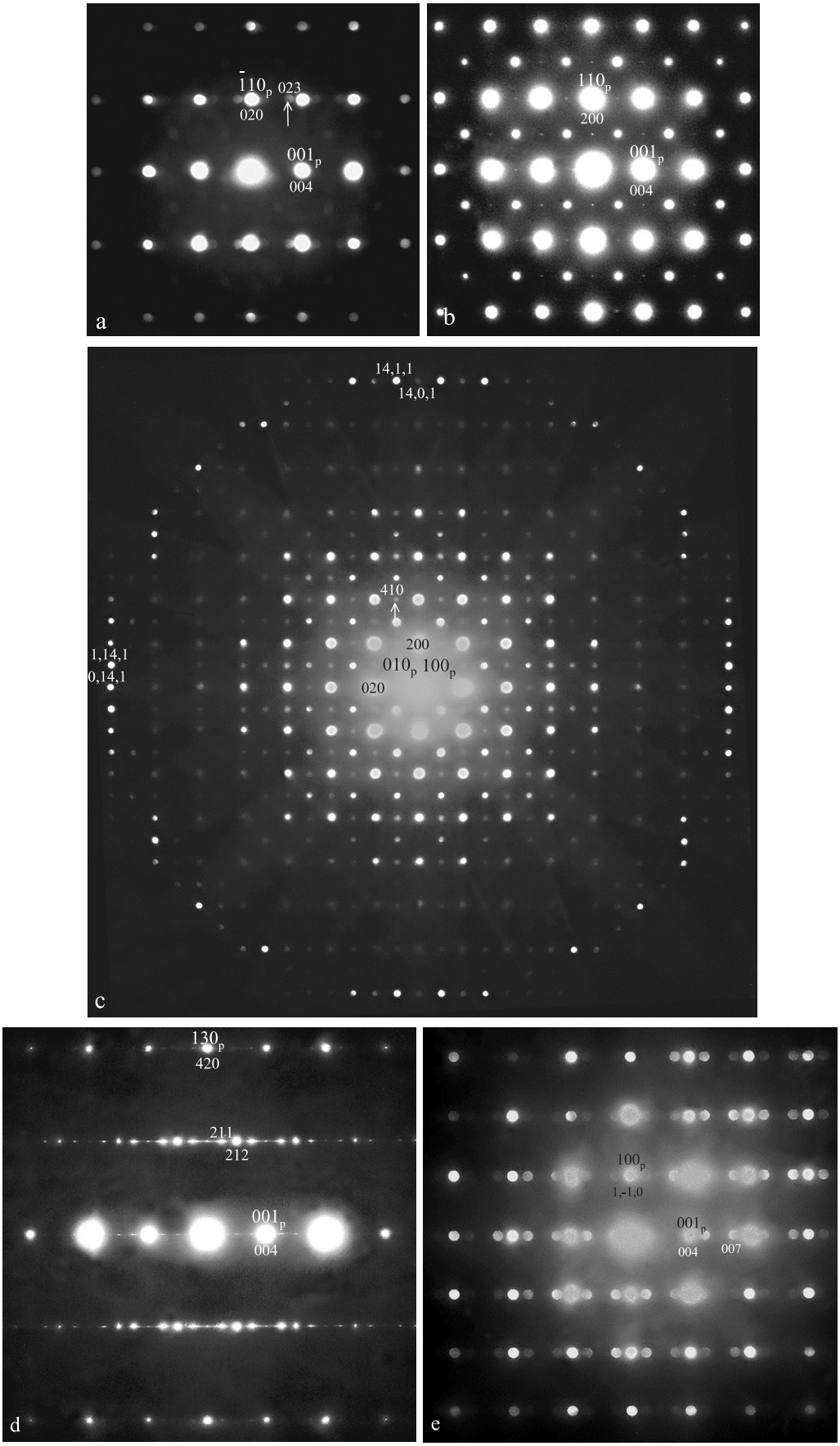

Figure 1. Single domain (b) [010], (c) [001], (d) [$\bar{1}$20] and (e) [110] zone axis EDP's of CST63. (a) Shows a very close to single domain [100] zone axis EDP. All EDP's are indexed both with respect to the true resultant unit cell as well as the underlying parent perovskite sub-structure, labelled with the subscript p. (a), (c) and (e) are micro-diffraction patterns taken with a focussed probe and a small condenser aperture.

for example Ti cation displacements and TiO_6 octahedral tilting relevant to the resultant structure. The primary distortions are associated with the modulation wavevectors $\mathbf{k} = [1/2, 1/2, 1/2]^*$ and $[1/2, 1/2, 1/4]^*$ and the induced or secondary distortions with $[0, 0, 1/4]^*$, $[1/2, 1/2, 0]^*$ and $[0, 0, 1/2]^*$ modulation wavevectors. The distortions in the refined structure are then decomposed to determine the amplitudes of these various different normal modes. The identification of the primary distortions is confirmed on the basis of the relative amplitudes of the modes thereby obtained.

We conclude with a discussion on what is a general softness in perovskites to octahedral tilting modes along the T ($\mathbf{k} = \langle 1/2, 1/2, \xi \rangle^*$) lines of the Brillouin zone. Although the vast majority of perovskites show tilting with $\xi = 0$ or $1/2$, $NaNbO_3$ in its P phase appears to be another perovskite which, like $Ca_{0.37}Sr_{0.63}TiO_3$, exhibits tilting with $\xi = 1/4$. This softening along the T line is quite evident through streaking in electron diffraction patterns from certain perovskites-or closely-related ReO_3 phases such as NbO_2F (Brink *et al* 2002).

2. Experimental details

2.1. Sample preparation

The $Ca_{0.37}Sr_{0.63}TiO_3$ sample was produced using the standard alkoxide/nitrate route (Ringwood *et al* 1988). The method involves the mixing of stoichiometric amounts of Ti isopropoxide with aqueous solutions of Sr and Ca nitrates, while continuously stirring. After thorough mixing and stir drying, the material was calcined in air at 750 °C for 1 h, and wet milled for 16 h using zirconia balls. The slurry was then dried at 110 °C overnight, and the dried clumps were ground in a mortar and pestle into fine powder. The powder was pressed into a 10 g pellet and sintered in air at 1550 °C for 96 h, then furnace cooled. A polished surface was carbon-coated and characterized by scanning electron microscopy (SEM), using a JEOL 6400 instrument fitted with a Tracor Northern energy dispersive spectrometer (EDS) operated at 15 kV. A comprehensive set of standards was used to calibrate the SEM/EDS, therefore giving a high degree of accuracy for quantitative work. This verified the expected $Ca_{0.37}Sr_{0.63}TiO_3$ composition and also showed the sample to be essentially homogeneous (a very small amount of rutile, <1%, was also detected). The $NaNbO_3$ sample was as supplied by Aldrich.

2.2. Electron diffraction

Given the very close to cubic metric symmetry of the underlying parent perovskite sub-structure of CST63 (see below), orientational faulting (twinning) as well as translational faulting (anti-phase boundaries) is only to be expected. Nevertheless, it was usually possible to obtain single domain electron diffraction patterns[5] (EDP's) either via careful positioning of the incident electron beam relative to the sample or through focussed probe micro-diffraction. Such EDP's unequivocally confirm the $\mathbf{a} = \mathbf{a}_p + \mathbf{b}_p$, $\mathbf{b} = -\mathbf{a}_p + \mathbf{b}_p$, $\mathbf{c} = 4\mathbf{c}_p$ ($\mathbf{a}^* = 1/2\ [110]^*_p$, $\mathbf{b}^* = 1/2\ [\bar{1}10]^*_p$, $\mathbf{c}^* = 1/4\ [001]^*_p$, p for parent perovskite sub-structure) unit cell. They also strongly suggest that the resultant space group symmetry is indeed *Pbcm*, as previously reported.

Figure 1, for example, shows single domain (b) [010], (c) [001], (d) $[\bar{1}20]$ and (e) [110] zone axis EDP's of CST63. Figure 1(a) shows a very, very close to single domain [100] zone axis EDP (a very faint trace of barely visible $\mathbf{G} \pm 1/2[\bar{1}11]^*_p$ reflections present in (a) suggest a tiny amount of a second orientational twin variant). All EDP's are indexed both with respect to the true resultant unit cell as well as the underlying parent perovskite sub-structure, labelled with the subscript p. Note that figures 1(a), (c) and (e) are, in fact, micro-diffraction patterns taken with a focussed probe (so that a much smaller area of specimen is illuminated than is the case for a conventional selected area EDP) and a small condenser aperture (so that the resultant convergent beam discs have a small diameter). The observed systematic extinctions are $F(0kl) = 0$ unless $k = 2J$, J an integer (see figure 1(a)) and $F(h0l) = 0$ unless $l = 2J$ (see figure 1(b)). No systematic extinction condition is observed in the zero order laue zone (ZOLZ) layer at the [001] zone axis orientation. The resultant space group symmetry is thus either $Pbc2_1$ or most probably *Pbcm* as previously suggested. Note that EDP's such as figures 1(a) and (b) were obtained by starting with EDP's such as those shown in (d) and (e) and then tilting around the $[001]^*$ systematic row taking care, as far as is possible, to make sure that the same area of specimen is illuminated.

Note that the $\mathbf{G} \pm 1/2[111]^*_p$ satellite reflections, such as e.g. $[212]^*$ in figure 1(d) are quite sharp with no trace of diffuse streaking along the $\mathbf{c}^*$ direction of reciprocal space whereas the $\mathbf{G} \pm [1/2, 1/2, 1/4]^*_p$ satellite reflections such as e.g. $[211]^*$, and indeed even the $\mathbf{G} \pm [00, 1/4]^*_p$ satellite reflections are clearly streaked out along the $\mathbf{c}^*$ direction of reciprocal space. This provides clear diffraction evidence for stacking fault disorder of the $\mathbf{k} = [1/2, 1/2, 1/4]^*_p$ and $[00, 1/4]^*_p$ modes of distortion along the $\mathbf{c}$ direction of real space. Selective peak broadening of these satellite reflections is also apparent in the neutron diffraction data (see below).

As far as the likely atomic displacement patterns associated with the various modes of distortion are concerned, consider the satellite reflections in the first order laue zone (FOLZ) ring of reflections in figure 1(c). Reflections in this first order laue zone (FOLZ) ring of reflections correspond to the next layer of reciprocal space up from the central, or Zero Order Laue Zone, layer i.e. to superlattice reflections of $[hk1]^*$ type. The ring of reflections is thus composed entirely of superlattice reflections. There are two such types of satellite reflections present in this FOLZ ring: (1) reflections of the type $\mathbf{G}_p \pm [1/2, 1/2, 1/4]^*_p$ such as the reflections labelled 14, 1, 1 and 1, 14, 1. The intensity distribution of these satellite reflections is essentially uniform around the FOLZ ring suggesting that they can only be associated with an octahedral rotation around [001] type mode. (This is also consistent with the absence of such reflections in the [100] and [010] zone axis EDP's shown in figures 1(a) and (b)). (2) reflections of the type $\mathbf{G}_p \pm [00, 1/4]^*_p$ such as the reflections labelled 14, 0, 1 and 0, 14, 1 in figure 1(c). Note the very strong difference in intensity between these latter two

[5] Making use of Philips EM 430 transmission electron microscope operating at 300 kV.

reflections i.e. 0, 14, 1 is quite strong whereas 14, 0, 1 is very weak. This modulation can therefore only be associated with a mode involving displacements primarily along the [010] direction. While one should in general be wary of over-interpreting intensity distributions in the central (or zero order laue zone) region of EDP's such as that shown in figure 1(c) (where multiple scattering effects are much more likely to be present), the observed intensity distribution of the $\mathbf{G}_p \pm 1/2[110]^*_p$ satellite reflections (such as the reflection labelled 410) again suggests that the $1/2[110]^*_p$ mode may also be associated with octahedral rotation around [001]. Finally note the complete absence of $\mathbf{G}_p \pm [00, 1/2]^*_p$ type satellite reflections in the [110] zone axis EDP shown in figure 1(e). This requires that the structural degrees of freedom associated with the $\mathbf{k} = [00, 1/2]^*_p$ modulation wavevector, while allowed by the resultant supercell and space group symmetry, must have very close to zero amplitude. Finally, the absence of the $\mathbf{G}_p \pm 1/2[111]^*_p$ satellite reflections at the [100] zone axis orientation is consistent with this large amplitude mode being associated with octahedral rotation around **b**.

2.3. Neutron diffraction

Neutron diffraction data were recorded, in the course of an extensive study of the $CaTiO_3$–$SrTiO_3$ system (Carpenter *et al* 2006), using the high resolution powder diffractometer, HRPD, at the ISIS neutron facility, Rutherford Appleton Laboratories, UK (Ibberson *et al* 1992). Detail on the experimental arrangement has been presented elsewhere (Carpenter *et al* 2006). Diffraction patterns were recorded over the time-of-flight range 30–130 ms, corresponding to a d-spacing range from 0.6 to 2.6 Å, or from 0.9 to 3.7 Å, for patterns collected in the back-scattering and ninety degree detector banks respectively. These patterns were normalized to the incident beam spectrum as recorded in the upstream monitor, and corrected for detector efficiency according to prior calibration with a vanadium scan. Measurements on $Ca_{0.37}Sr_{0.63}TiO_3$ were made first at room temperature, then in the cryostat at 4.2 K, 10 K, and at 10 K intervals to 400 K, and finally in the furnace. Measurements at 4.2 K and at room temperature were made to a total incident proton beam of at least 100 μA h, corresponding to about 3 h data collection, and these provide the neutron data considered here. At other temperatures, diffraction patterns were recorded only to about 10 μA h incident proton beam. They were sufficient nevertheless to show a first order transition occurring over the temperature range 320–340 K, from the *Pbcm* phase, of interest here, to the more commonly observed tetragonal structure in $I4/mcm$ (Carpenter *et al* 2006).

Figure 2 shows an extract, for the d-spacing range from 1.55 to 2.5 Å, from the 4.2 K diffraction pattern as recorded in the back-scattering detector bank. The extract is shown on an expanded vertical scale, so as to highlight the superlattice reflections of interest in this work. Peaks have been indexed by reference to the parent perovskite cell, so peaks with all integral indices are from the parent perovskite sub-structure. The superlattice peaks have been labelled R, T, Δ, M or X according as they index as $\mathbf{G}_p \pm 1/2[111]^*_p$, $\mathbf{G}_p \pm [1/2, 1/2, 1/4]^*_p$, $\mathbf{G}_p \pm [00, 1/4]^*_p$, $\mathbf{G}_p \pm 1/2[110]^*_p$ or

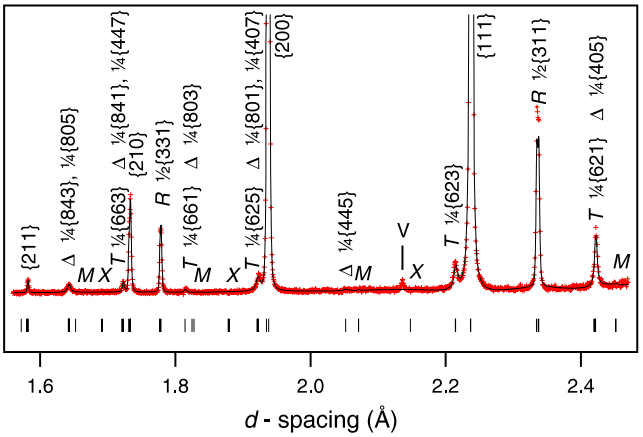

Figure 2. Extract ($1.55 < d < 2.5$ Å) from the diffraction pattern recorded in the back-scattering detectors from $Ca_{0.37}Sr_{0.63}TiO_3$ at 4.2 K. Crosses represent the observed data, and the continuous line shows a fit obtained by the Rietveld method. The markers below the pattern indicate the positions of reflections allowed by the structure assumed, space group symmetry *Pbcm*, and these have been re-indexed in reference to the perovskite parent subcell. Peaks marked with integral indices arise from the underlying parent sub-structure, whereas the other peaks, with fractional indices, are labelled R, T, Δ, M and X, see text. The feature marked V is attributed to vanadium in the sample container.

$\mathbf{G}_p \pm [00, 1/2]^*_p$ respectively. Consistent with the electron diffraction, the neutron pattern shows peaks at the R-points that are relatively strong and sharp, peaks corresponding to T and Δ that are measurable but show some broadening, and very little if any intensity at the M- or X-point reflections. The M-point, $\mathbf{G}_p \pm 1/2[110]^*_p$, superlattice reflections can be discerned as weak reflections in the EDP's (see again figure 1(c), reflection labelled 410), but evidently too weak to appear in the neutron pattern. There is no sign of intensities at the X-points, $\mathbf{G}_p \pm [00, 1/2]^*_p$, in patterns of either type. All observed reflections in the neutron pattern are consistent with the *Pbcm* space group symmetry hitherto assumed.

Structure refinements were carried out, at 4.2 K and room temperature, making use of the recorded neutron data, and assuming both *Pbcm* symmetry and the $\sqrt{2}a_p \times \sqrt{2}a_p \times 4a_p$ unit cell. These refinements were undertaken using the Rietveld method as implemented in the GSAS computer program (Rietveld 1969, Larson and Von Dreele 2004, Toby 2001). Starting structures could have been taken from previous publications (Mishra *et al* 2002, 2006) but were in fact obtained simply by setting the parent perovskite structure into the $\sqrt{2}a_p \times \sqrt{2}a_p \times 4a_p$ unit cell[6], then displacing one oxygen atom from its starting position. Patterns from the back-scattering and ninety degree banks were fitted simultaneously, the diffractometer constant for the ninety degree bank being released to allow optimum matching of the patterns. Peak shape was modelled as the convolution of back to back exponentials with a pseudo-Voigt function in which two (σ_1, γ_1) or, for the ninety degree bank, three (σ_1, σ_2, γ_1) peak width

[6] This aided by computer program ISOTROPY (Stokes *et al* 2007), which takes account of the necessary origin shift.

Table 1. Crystal structure of $Ca_{0.37}Sr_{0.63}TiO_3$ at 4.2 K and at room temperature.

Atom	x	y	z	U_{iso} (10^{-2} Å^2)
$T = 4.2$ K, space group *Pbcm*, $a = 5.482\,75(7)$, $b = 5.481\,08(7)$, $c = 15.478\,25(10)$ Å $R^a_{wp} = 5.3, 2.9\%$, $R_B = 6.7, 1.9\%$				
Ca/Sr1	0.2464(10)	0.75	0	0.48(9)
Ca/Sr2	0.2486(7)	0.7299(6)	0.25	0.23(8)
Ti	0.2491(20)	0.2412(9)	0.1248(8)	0.19(3)
O1	0.2105(10)	0.25	0	0.69(14)
O2	0.2984(11)	0.2560(9)	0.25	0.77(16)
O3	−0.0237(7)	0.4778(7)	0.1361(2)	0.53(8)
O4	0.5214(7)	0.0237(7)	0.1145 (2)	0.35(8)
$T = 293$ K, space group *Pbcm*, $a = 5.492\,15(7)$, $b = 5.488\,69(6)$, $c = 15.509\,44(12)$ Å $R_{wp} = 6.5, 4.6\%$, $R_B = 8.4, 3.1\%$				
Ca/Sr1	0.2455(12)	0.75	0	0.85(8)
Ca/Sr2	0.2515(11)	0.7388(8)	0.25	0.70(8)
Ti	0.2492(14)	0.2480(11)	0.1243(8)	0.22(2)
O1	0.2144(10)	0.25	0	1.01(14)
O2	0.2952(10)	0.2522(12)	0.25	1.13(16)
O3	−0.0196(7)	0.4824(8)	0.1351(3)	0.80(12)
O4	0.5162(7)	0.0169(8)	0.1151(2)	0.69(12)

[a] There are two entries for each measure of fit, the first referring to fitting the pattern in the back-scattering detectors, and the second to the ninety degree bank.

parameters were varied (Larson and Von Dreele 2004). The GSAS 'stacking fault' option was invoked to define a subset, *hkl* with l even, of unaffected reflections, then to allow additional broadening (via parameter γ_{2s}) of the remainder (reflections with l odd, comprising those characterized as Δ and T). Backgrounds in the back-scattering and ninety degree banks were modelled by 24 and 10 term shifted Chebyshev polynomials respectively. Internal coordinates were refined along with isotropic displacement parameters. Calcium and strontium were taken to be distributed randomly on their shared sites, and on each such site their positions and displacement parameters constrained to be equal. The results from these refinements are recorded in table 1, while the extract in figure 2 illustrates the quality of the fits.

Two views of the refined structure, at 4.2 K, are shown in figure 3. The main features are tilting of the TiO_6 octahedra around an axis parallel to $[\bar{1}10]_p$, which is the y-axis in *Pbcm*, and also around $[001]_p$, the z-axis in *Pbcm*, such that two octahedra tilt in one sense and the next two in the opposite sense. The angle of tilt around the y-axis can be estimated either from the displacement of the apical oxygen atoms, O1 and O2, using $\tan\phi = \sqrt{2}(x(O2) - x(O1))$ or from the positions of the equatorial oxygen atoms, O3 and O4, using $\tan\phi = 4\sqrt{2}(z(O3) - z(O4))$. These two estimates are consistent provided $x(O2) - x(O1) = 4(z(O3) - z(O4))$, which we find to be very nearly the case. The angle of tilt around the z-axis is estimated from the positions of the equatorial oxygens, using $\tan\psi = x(O4) + y(O4) - x(O3) - y(O3)$. The tilts at 4.2 K (293 K) are thus 7.0° (6.5°) around the y-axis, and 5.2° (4.0°) around the z-axis. There is also a small but significant displacement of the Ti atoms along the y-axis, from $y = 1/4$, amounting at 4.2 K (293 K) to 0.05 Å (0.01 Å).

We present in the next section a more formal analysis of the various possible distortion modes, and determine the amplitude of each. This will confirm the above assertions as to the nature of the major distortions. The decomposition into the different modes will also provide a convenient means to compare our results on this structure with those previously published (Mishra *et al* 2002, 2006, Daniels *et al* 2006). In addition, by identifying and ascribing zero amplitude to the mode associated with the X-points, $\mathbf{G}_p \pm [00, 1/2]^*_p$, where no intensities are observed, it becomes possible to repeat the refinements with the constraints $z(Ti) = 1/8$, and $z(O3) + z(O4) = 1/4$.

3. Normal mode analysis

Enumeration of the possible modes of distortion of the ideal perovskite, and the decomposition of the distortions observed in the derivative structures, are lengthy operations whatever

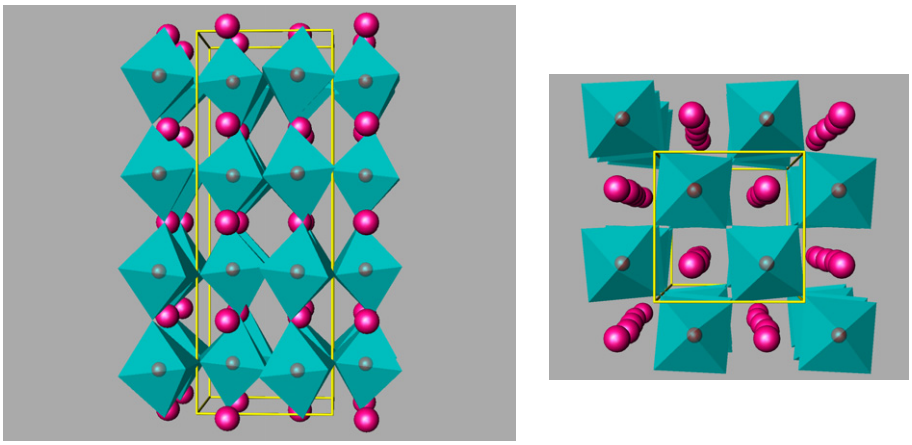

Figure 3. Two views of the structure of $Ca_{0.37}Sr_{0.63}TiO_3$ at 4.2 K, drawn using the program ATOMS (Dowty 2003) from the coordinates listed in table 1. The first is a view along the y-axis, parallel to $[\bar{1}10]_p$, and the tilting of the TiO_6 octahedra around axes in this direction can be quite clearly seen. The second is a view down the z-axis, $[001]_p$. This view shows tilting around this direction, octahedra in the top two layers tilting in one sense and octahedra in the two layers beneath them in the opposite sense.

Table 2. The displacements of atoms affected by modes associated with the different irreps. The starting atomic positions shown are those of the undistorted perovskite, but referred to the *Pbcm* cell. The entries in the tables present the effects on atomic coordinates as multipliers of the amplitudes (in units of the $Pm\bar{3}m$ cell edge) of the different modes. Note that there are, associated with irrep Δ_5, three independent modes causing oxygen atom displacements.

	Ca/Sr1 on 4c, $(1/4+\Delta x, 3/4, 0)$	Ca/Sr2 on 4d, $(1/4+\Delta x, 3/4+\Delta y, 1/4)$	
	Δx	Δx	Δy
Δ_5	—	—	$-1/\sqrt{2}$
R_5^+	$1/\sqrt{2}$	$-1/\sqrt{2}$	—
M_5^-	$1/\sqrt{2}$	$1/\sqrt{2}$	—

	Ti on 8e, $(1/4+\Delta x, 1/4+\Delta y, 1/8+\Delta z)$		
	Δx	Δy	Δz
Δ_5	—	$-1/\sqrt{2}$	—
X_3^-	—	—	$-1/4$
M_5^-	$-1/\sqrt{2}$	—	—

	O1 on 4c, $(1/4+\Delta x, 1/4, 0)$	O2 on 4d, $(1/4+\Delta x, 1/4+\Delta y, 1/4)$		O3 on 8e, $(\Delta x, 1/2+\Delta y, 1/8+\Delta z)$			O4 on 8e, $(1/2+\Delta x, \Delta y, 1/8+\Delta z)$		
	Δx	Δx	Δy	Δx	Δy	Δz	Δx	Δy	Δz
$\Delta_5(1)$	—	—	—	1/2	$-1/2$	—	1/2	$-1/2$	—
$\Delta_5(2)$	—	—	—	1/2	1/2	—	1/2	1/2	—
$\Delta_5(3)$	—	—	$-1/\sqrt{2}$	—	—	—	—	—	—
R_4^+	$1/\sqrt{2}$	$-1/\sqrt{2}$	—	—	—	$-1/(4\sqrt{2})$	—	—	$1/(4\sqrt{2})$
R_5^+	$-1/\sqrt{2}$	$1/\sqrt{2}$	—	—	—	$-1/(4\sqrt{2})$	—	—	$1/(4\sqrt{2})$
X_3^-	—	—	—	—	—	$-1/4$	—	—	$-1/4$
M_5^-	$1/\sqrt{2}$	$1/\sqrt{2}$	—	—	—	—	—	—	—
T_2	—	—	—	$-1/2$	1/2	—	1/2	$-1/2$	—
T_4	—	—	—	$-1/2$	$-1/2$	—	1/2	1/2	—

approach is used. Here we present, in outline only, an analysis making use of group theory as implemented in the ISOTROPY computer program (Stokes *et al* 2007). The more general application of this program to the study of perovskite structures was the subject of a recent review (Howard and Stokes 2005).

We remark that the decomposition presented here was carried out manually in the first instance, with identical results.

We start from the ideal perovskite structure, cubic with space group symmetry $Pm\bar{3}m$, and the premise (to be justified shortly) that the primary distortions are octahedral tilts. Each of these distortions will be associated with an irreducible representation (irrep) of the parent space group, the irreps being labelled according to the notation of Miller and Love (1967). One of the primary distortions is out-of-phase tilting of the TiO_6 octahedra associated with the irreducible representation (irrep) $R_4^+(\mathbf{k} = [1/2, 1/2, 1/2]^*)$. This can produce tilting of the octahedra around $[\bar{1}10]_p$ and a structure with space group symmetry *Ibmm* on a $\sqrt{2}a_p \times \sqrt{2}a_p \times 2a_p$ unit cell. The other primary distortion, in our view, is the unusual tilt pattern wherein two successive octahedra tilt in one sense and the next two in the opposite sense. This leads by itself to a quadrupling of the parent unit cell along one of its axes, and a doubling along the other two. The distortion is associated thus with the point $\xi = 1/4$ on the T line of symmetry $\mathbf{k} = [1/2, 1/2, \xi]^*$. Following Howard and Stokes (2005), we use ISOTROPY to determine that the only irreps leading to any tilting of the TiO_6 octahedra (that is, around Wyckoff position *a* in $Pm\bar{3}m$) are T_4 and T_5. Close inspection of the ISOTROPY output reveals that only T_4 leads to a tilting pattern in which adjacent octahedra in a plane perpendicular to the tilt axis have opposite sign, as required to maintain their corner connectivity. The required tilting pattern is indeed produced by irrep T_4, in a structure with space group symmetry $I4/mcm$ on a $\sqrt{2}a_p \times \sqrt{2}a_p \times 4a_p$ unit cell. The irreps having been identified, ISOTROPY can be used to list the different structures that can arise from their combination, and this list indeed includes the structure we find, in space group *Pbcm*, with origin and basis vectors referred to the $Pm\bar{3}m$ parent being 0, 1/2, 1/2, and 1, 1, 0, $\bar{1}$, 1, 0, 0, 0, 4 respectively.

The next step is to examine the lower symmetry *Pbcm* structure relative to the $Pm\bar{3}m$ parent to see what distortions other than the two (assumed) primary distortions might be allowed. This examination is undertaken simply by entering the parent and subgroup symmetries, and the lattice vectors of the subgroup referred to the parent group (as shown above) into ISOTROPY, or more specifically into COPL (Complete Order Parameter Listing, see Stokes *et al* 2007, Hatch and Stokes 2001). The program lists, along with what we have taken to be the primary distortions (irreps R_4^+ and T_4), additional distortions associated with irreps Γ_1^+, Γ_3^+, $\Gamma_5^+(\mathbf{k} = [0, 0, 0]^*)$, $R_5^+(\mathbf{k} = [1/2, 1/2, 1/2]^*)$, $T_2(\mathbf{k} = [1/2, 1/2, 1/4]^*)$, $\Delta_5(\mathbf{k} = [0, 0, 1/4]^*)$, $M_5^-(\mathbf{k} = [1/2, 1/2, 0]^*)$, X_2^- and $X_3^-(\mathbf{k} = [0, 0, 1/2]^*)$. Finally, ISOTROPY is used to evaluate the displacements associated with each of the irreps at the positions (Wyckoff positions a, b, d) occupied in the parent $Pm\bar{3}m$ structure. ISOTROPY shows atomic positions and displacements relative to the $Pm\bar{3}m$ structure; for our purpose they are rewritten to refer to the lattice vectors

Table 3. Description of the *Pbcm* structure of $Ca_{1-x}Sr_xTiO_3$ as a distorted variant of the ideal perovskite, in terms of amplitudes of normal modes. The modes are labelled according to their association with the irreps of $Pm\bar{3}m$. Entries in this table have been checked directly using program ISODISPLACE (Campbell *et al* 2006).

	$\Delta_5(1)$	$\Delta_5(2)$	$\Delta_5(3)$	R_4^+	R_5^+	X_3^-	M_5^-	T_2	T_4
$Ca_{0.37}Sr_{0.63}TiO_3$ at 4.2 K—this work									
Ca/Sr	0.0284				−0.0016		−0.0035		
Ti	0.0124					0.0008	0.0013		
O	−0.0019	−0.0004	−0.0085	−0.0616	0.0005	−0.0012	0.0063	−0.0004	0.0455
$Ca_{0.37}Sr_{0.63}TiO_3$ at 293 K—this work									
Ca/Sr	0.0158				−0.0042		−0.0021		
Ti	0.0028					0.0028	0.0011		
O	−0.0014	−0.0021	−0.0031	−0.0569	0.0003	−0.0004	0.0068	0.0007	0.0352
$Ca_{0.25}Sr_{0.75}TiO_3$ at 102 K (Mishra *et al* 2002)—neutron diffraction									
Ca/Sr	−0.0156				0.0078		0.0007		
Ti	−0.0071					−0.0040	0.0028		
O	0.000	0.0040	−0.0099	0.0525	0.0001	−0.0020	−0.0057	0.0020	0.0200
$Ca_{0.40}Sr_{0.60}TiO_3$ at 300 K (Mishra *et al* 2006)—x-ray diffraction									
Ca/Sr	−0.0104				0.0076		0.0008		
Ti	−0.0146					0.0052	−0.0016		
O	−0.006	0.009	0.0038	0.0572	0.0152	0.0008	−0.0165	−0.0066	0.0344
$Ca_{0.3}Sr_{0.7}TiO_3$ at 8 K (Daniels *et al* 2006)—neutron diffraction									
Ca/Sr	−0.0014				−0.0177		0.0035		
Ti	0.0014					−0.0120	−0.0085		
O	−0.0005	0.0015	−0.0157	0.0474	−0.0050	0.0020	−0.0113	−0.0085	0.0275

and origin of *Pbcm*. It is found that irreps Γ_1^+, Γ_3^+ and Γ_5^+ have no impact on any atomic coordinates (these irreps correspond to macroscopic strains), while irrep X_2^- has no effect at the particular positions that are occupied. The modes corresponding to the remaining irreps effect displacements of the different atoms as indicated in table 2.

Table 2 provides in effect a set of matrices that transform from the amplitudes of the normal modes to the variable position coordinates in the structure. There being the same number of degrees of freedom in either description the matrices are necessarily square and indeed non-singular. The inverse matrices can be used to effect the reverse transformation, that is from atomic displacements as reckoned from the observed structure (positions recorded in table 1 relative to the ideal positions shown as the starting positions in table 2) to normal mode amplitudes. This will be the decomposition we seek. Table 2 also provides the basis for our earlier remark that the lack of intensity at the X-points could be used to introduce additional constraints: taking the amplitude of the mode associated with X_3^- to be zero would imply both $\Delta z(\mathrm{Ti}) = 0$ and $\Delta z(\mathrm{O3}) = -\Delta z(\mathrm{O4})$ and thus the suggested constraints. The difficulty of observing the M-point reflections, at least in the neutron pattern, suggests the possibility of invoking other constraints, for example $\Delta x(\mathrm{O1}) = -\Delta x(\mathrm{O2})$, $x(\mathrm{O1}) + x(\mathrm{O2}) = 1/2$. We have however not employed these constraints in the refinements reported here.

The results of our decomposition are presented in table 3. We have completed this decomposition not only for our own structures of $Ca_{0.37}Sr_{0.63}TiO_3$ at 4.2 and 293 K (table 1), but also for the published structures of $Ca_{0.25}Sr_{0.75}TiO_3$ at 102 K (Mishra *et al* 2002), $Ca_{0.4}Sr_{0.6}TiO_3$ at 300 K (Mishra *et al* 2006), and $Ca_{0.3}Sr_{0.7}TiO_3$ at 8 K (Daniels *et al* 2006).

The data recorded in this table are seen to confirm our premise that the most significant distortions are the octahedral tilting modes associated with irreps R_4^+ and T_4, the amplitudes at 4.2 K being 0.0616 and 0.0455 respectively. The data also indicate smaller but significant displacements of the cations Ca/Sr and Ti (amplitudes 0.0284 and 0.0124 at 4.2 K) associated with irrep Δ_5. The amplitudes of all these modes are smaller at room temperature. It is clear from the table that in setting our structure we have selected the same sign as Mishra *et al* (2002, 2006) and Daniels *et al* (2006) for the T_4 mode, but opposite signs for the modes associated with R_4^+ and $\Delta_5(1)$.[7] Making allowance for this, it can be seen there is good agreement as regards the two tilting modes (R_4^+ and T_4) between the two structure determinations at room temperature, even though the compositions were slightly different. The amplitudes of these modes are smaller for the 102 and 8 K structure determinations on samples of rather different composition. The earlier structures show larger amplitudes than ours for modes associated with irrep X_3^-, whereas our measurements show directly that the amplitude of this mode should be effectively zero. We also believe there is a problem with the x-ray determination and perhaps with the most recent neutron determination (Daniels *et al* 2006) in that they show rather large M-point amplitudes affecting the oxygen, whereas we can find no M-point intensities in

[7] Shifting the origin by $[102]_p$, for example, would cause a sign change in table 3 of the R, Δ and M modes, leaving the signs of the T and X modes unchanged.

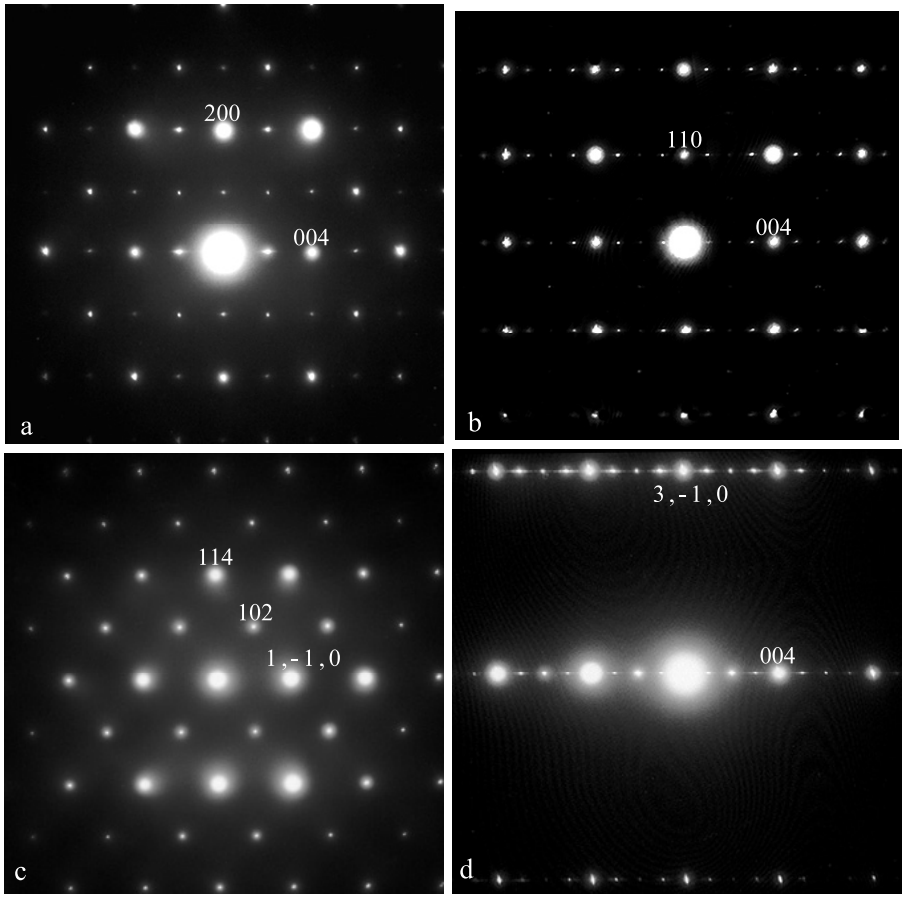

Figure 4. Single domain (a) [010], (b) [1$\bar{1}$0], (d) [22$\bar{1}$] and (e) [130] zone axis EDP's of the P phase of $NaNbO_3$. All EDP's are indexed with respect to a $\sqrt{2}a_p \times \sqrt{2}a_p \times 4a_p$ unit cell.

our neutron diffraction. Based on this analysis, together with the quality of high resolution neutron data (cf Mishra *et al* 2002, medium resolution only), we consider the coordinates we report here to be significantly more precise and reliable than those published previously.

4. Relationship to $NaNbO_3$

The structure just described, having space group symmetry *Pbcm* and on a $\sqrt{2}a_p \times \sqrt{2}a_p \times 4a_p$ cell, was proposed much earlier for the room temperature form of $NaNbO_3$ (Megaw and Wells 1958, Sakowski-Cowley *et al* 1969). Ranjan *et al* (2000) indeed proposed the *Pbcm* structure in $CaTiO_3$–$SrTiO_3$ as being similar to that $NaNbO_3$ structure after observing superlattice reflections in the low temperature x-ray pattern from $Ca_{0.3}Sr_{0.7}TiO_3$ that could be indexed only on the larger unit cell.

To further investigate the analogy between the *Pbcm* structure in $CaTiO_3$–$SrTiO_3$, for example at $Ca_{0.37}Sr_{0.63}TiO_3$ and the room temperature structure of $NaNbO_3$, we recorded electron diffraction patterns from the *P* phase of $NaNbO_3$, shown here in figure 4. The EDP's could be indexed in the same manner as $Ca_{0.37}Sr_{0.63}TiO_3$ on a $\sqrt{2}a_p \times \sqrt{2}a_p \times 4a_p$ unit cell. The figure shows (a) [010] (b) [1$\bar{1}$0] (c) [22$\bar{1}$] and (d) [130] zone axis EDP's. Once again the [010] zone axis pattern shows the systematic extinction $F(h0l) = 0$ unless $l = 2J$, requiring a *c*-glide perpendicular to **b**. Unfortunately, a single domain [100] zone axis pattern to confirm the existence of a *b*-glide perpendicular to **a** was not obtained. Nonetheless, the EDP's obtained are remarkably similar to those obtained from $Ca_{0.37}Sr_{0.63}TiO_3$, and again space group *Pbcm* is indicated. As for CST63, the $\mathbf{G} \pm [00, 1/4]^*_p$ and presumably the $\mathbf{G} \pm [1/2, 1/2, 1/4]^*_p$ satellite reflections are streaked out along the $\mathbf{c}^*$ direction of reciprocal space. One minor difference is that reflections such as 002 in figure 4(b) ($\mathbf{G}_p \pm [00, 1/2]^*_p$, *X*-points) which were space group allowed but not seen in $Ca_{0.37}Sr_{0.63}TiO_3$ are visible here.

Three sets of refined coordinates for the room temperature structure of $NaNbO_3$, assumed to have space group symmetry *Pbcm*, appear in the literature. The first comes from the original single crystal x-ray study of Sakowski-Cowley *et al* (1969). This seems to be quite careful work. The second comes from a relatively early application of the Rietveld method to neutron powder data of modest resolution (Hewat 1974). The third is a modern result (Xu *et al* 2003), based again on Rietveld fitting to a neutron powder pattern. By the same methods as in section 3, we have taken the published results and decomposed the distortions away from the ideal perovskite structure into normal modes, to facilitate comparison of these results one with another and also with the *Pbcm* structure in $CaTiO_3$–$SrTiO_3$. The results from these decompositions

Table 4. Description of the room temperature structure of $NaNbO_3$ as a distorted variant of the ideal perovskite, in terms of amplitudes of normal modes. The modes are labelled as in table 3.

	$\Delta_5(1)$	$\Delta_5(2)$	$\Delta_5(3)$	R_4^+	R_5^+	X_3^-	M_5^-	T_2	T_4
Sakowski-Cowley *et al* (1969)-single crystal x-ray diffraction									
Na	−0.0452				0.0028		−0.0127		
Nb	−0.0314					−0.0048	−0.0093		
O	0.0015	0.0005	0.0240	0.0824	0.0025	0.0000	−0.0035	0.0025	0.0675
Hewat (1974)-neutron powder diffraction									
Na	−0.0438				0.0021		0.0078		
Nb	−0.0290					0.0076	0.0042		
O	0.0080	−0.0110	0.0255	0.0891	0.0014	0.0000	−0.0113	0.0000	0.0690
Xu *et al* (2003)-neutron powder diffraction									
Na	0.0099				−0.0042		−0.0184		
Nb	−0.0117					−0.0040	0.0054		
O	−0.0137	0.0461	0.0139	0.0874	−0.0040	0.0002	−0.0052	−0.0099	0.0661
Knight (unpublished data)-neutron powder diffraction									
Na	−0.0484				−0.0010		0.0234		
Nb	−0.0265					−0.0005	0.0043		
O	0.0121	−0.0202	0.0343	0.0873	0.0004	0.0021	−0.0012	−0.0003	0.0738

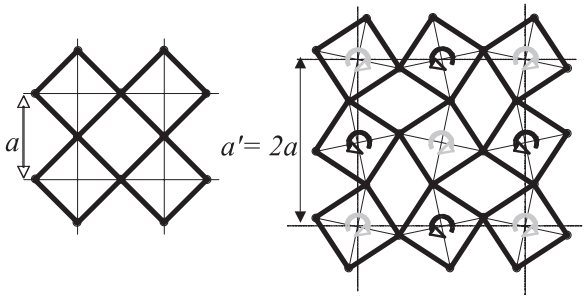

Figure 5. Shows the ideal BO_3 octahedral framework in projection along an ⟨001⟩ direction on the left and an octahedrally rotated framework on the right. Note that octahedral tilting around say [001] automatically doubles the periodicity along the orthogonal [100] and [010] directions and that once one octahedron is tilted then the sense of rotation of all the octahedra in the layer is determined.

are collected in table 4. In addition, we have a preliminary refinement from high resolution neutron data obtained using HRPD. The patterns recorded, like earlier ones recorded by the same instrument (Darlington and Knight 1999), show an unexplained broadening of the $\{100\}_p$ peaks. Nevertheless, we have in our preliminary refinement made the usual assumption of the structure in space group *Pbcm*, and the fits obtained were reasonably satisfactory. The mode amplitudes obtained from decomposing the results from our preliminary refinement have also been included in table 4.

It can be seen from this analysis (or directly from the published data) that the results obtained by Hewat (1974) are in excellent agreement with those of Sakowski-Cowley *et al* (1969), and also in very good agreement with those from Knight (unpublished). Evidently, the oxygen displacements are dominated in this compound too by the octahedral tilting modes associated with the irreps R_4^+ and T_4. The amplitudes of these modes for $NaNbO_3$ at room temperature (∼0.0824, 0.0675) are indeed somewhat larger than the corresponding amplitudes in $Ca_{0.37}Sr_{0.63}TiO_3$ at 4.2 K (0.0616, 0.0455)-the tilt angles for the NbO_6 octahedra are 9.3° around the *y*-axis (associated with R_4^+) and 7.7° around the *z*-axis (T_4). The cations Na and Nb show significant displacement associated with irrep $\Delta_5(1)$, the amplitudes (0.0452, 0,0314) being comparable with those of the tilting modes. The structure as described by Xu *et al* is somewhat different from the other two-the octahedra show significant amplitudes (0.0874, 0.0661) in the tilting modes as for the other results, but also large, and in our view problematic, distortion modes associated with irrep Δ_5. On the other hand the cation displacements associated with irrep $\Delta_5(1)$ are substantially smaller than those in the other reports.

5. Discussion and conclusions

Our studies of CST63, as well as the various studies of $NaNbO_3$ described above, serve to highlight a general softness of perovskites along the *T* line of symmetry. Ideal ABO_3 perovskites are characterized by a corner-connected BO_3 octahedral framework structure shown in projection along an ⟨001⟩ direction in figure 5. If we rotate one of the octahedra in this framework around ⟨001⟩ about an axis running through the apical oxygen atoms and the *B* atom in the centre of the octahedron then all the remaining octahedra in the {001} layer are automatically constrained to rotate as shown on the right-hand side of figure 5. Such a rotation automatically doubles the periodicity along the orthogonal [100] and [010] directions. Note, however, that it does not determine the sense of rotation from one {001} octahedral layer to the next. In soft mode terms, rotation around ⟨001⟩ is automatically associated with a modulation wavevector of $\langle 1/2, 1/2, \xi\rangle^*$ where ξ could, in principle, be anything. In practice, Glazer and all subsequent authors, when listing the possible subgroups of the ideal $Pm\bar{3}m$ parent perovskite structure derived from

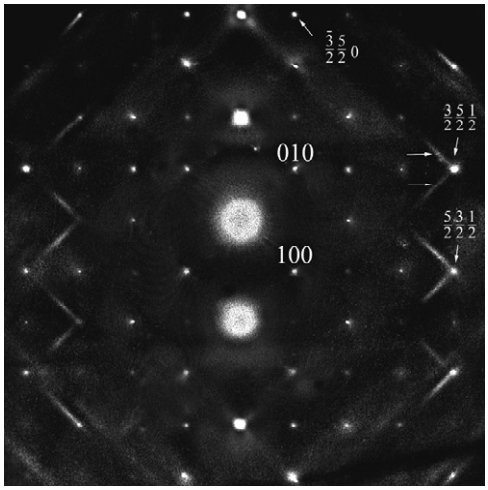

Figure 6. Selected area EDP from NbO_2F taken close to a ⟨118⟩ orientation (within ∼10° of an ⟨001⟩ zone axis orientation). Note the apparent 'satellite reflections' at $1/2[351]^*$ and $1/2[\bar{3}50]^*$ (arrowed) as well as the extended diffuse streaking (horizontal arrows) emanating from $\mathbf{G} \pm 1/2[351]^*$ along the $[100]^*$ and $[010]^*$ directions of reciprocal space.

octahedral tilting have assumed that ξ can only take the value 0 or 1/2. This severely limits the number of possible derivative structures. In practice, this assumption has proved to be pretty reasonable and almost always the case. The significance of the current work is that it provides the first example of mode decomposition for a well-refined perovskite-related structure involving significant octahedral tilting characterized by $\xi \neq 0$ or 1/2, in this case $\xi = 1/4$.

Note that rotation around [100] should be characterized by modulation wavevectors $[\xi, 1/2, 1/2]^*$, rotation around [010] by modulation wavevectors $[1/2, \xi, 1/2]^*$ and rotation around ⟨001⟩ by a modulation wavevector of $[1/2, 1/2, \xi]^*$. One might then expect to observe diffuse rods of intensity running along the $\langle 001\rangle^*$ directions of reciprocal space at $\mathbf{G} \pm \langle 1/2, 1/2, \xi\rangle^*$ in the high temperature cubic forms of perovskites. These three rods of diffuse intensity should intersect at the $\mathbf{G} \pm \langle 1/2, 1/2, 1/2\rangle^*$ regions of reciprocal space. This has, in fact, been observed in the case of the ReO_3 type[8], NbO_2F phase (see figure 6, taken from Brink *et al* 2002). Figure 6 was obtained by tilting ∼10° away from an ⟨001⟩ zone axis orientation to bring up $\mathbf{G} \pm \langle 1/2, 1/2, 1/2\rangle^*$ reflections (two are labelled in figure 6). Note the diffuse streaking emanating from these 'reflections' along the $\langle 100\rangle^*$ and $\langle 010\rangle^*$ directions of reciprocal space. The third such rod of diffuse intensity is coming out of the paper towards the reader.

The occurrence of specific examples of well-refined perovskite phase, such as CST63 and $NaNbO_3$, showing octahedral tilting modes with ($\mathbf{k} = [1/2, 1/2, \xi]^*$), $\xi \neq 0$ or 1/2, suggests that the well-known family tree of possible perovskite-related derivative structures (Glazer 1972, Howard and Stokes 2005) is far from complete and raises the intriguing possibility of many more such perovskite-related derivative structures being discovered in the future.

[8] The reader is reminded that the ReO_3 structure is in effect a perovskite lacking the *A* cation.

Acknowledgments

The preliminary refinement of the room temperature structure of $NaNbO_3$ (Knight, unpublished, in table 4) was carried out using data kindly made available by Knight and co-workers. Travel by CJH and ZZ to ISIS was funded by the Commonwealth of Australia under the Access to Major Research Facilities Program. Studies of perovskites are currently supported by the Australian Research Council, grant DP055722 (CJH and RLW).

References

Brink F J, Withers R L and Noren L 2002 An electron diffraction and crystal chemical investigation of oxygen/fluorine ordering in niobium oxyfluoride, NbO_2F *J. Solid State Chem.* **166** 73–80

Campbell B J, Stokes H T, Tanner D E and Hatch D M 2006 ISODISPLACE: a web-based tool for exploring structural distortions *J. Appl. Crystallogr.* **39** 607–14

Carpenter M A, Howard C J, Knight K S and Zhang Z 2006 Structural relationships and a phase diagram for (Ca, Sr) TiO_3 perovskites *J. Phys.: Condens. Matter* **18** 10725–49

Daniels J E, Elcombe M M, Finlayson T R and Vance E R 2006 Neutron diffraction study of polycrystalline $Ca_{1-x}Sr_xTiO_3$ mixed perovskite materials *Physica* B **385/386** 88–90

Darlington C N W and Knight K S 1999 On the lattice parameters of sodium niobate at room temperature and above *Physica* B **266** 368–72

Dowty E 2003 *ATOMS Version 6.0* (Kingsport Tennessee, USA: Shape Software) www.shapesoftware.com

Glazer A M 1972 Classification of tilted octahedra in perovskites *Acta Crystallogr.* B **28** 3384–92

Hatch D M and Stokes H T 2001 Complete listing of order parameters for a crystalline phase transition—a solution to the generalized inverse Landau problem *Phys. Rev.* B **65** 014113

Hewat A W 1974 Neutron powder profile refinement of ferroelectric and antiferroeletric crystal structures–sodium niobate at 22 °C *Ferroeletrics* **7** 83–5

Howard C J and Stokes H T 2005 Structures and phase transitions in perovskites—a group theoretical approach *Acta Crystallogr.* A **61** 93–111

Ibberson R M, David W I F and Knight K S 1992 The high resolution neutron powder diffractometer (HRPD) at ISIS—a user guide *Report RAL* 92-031

Larson A C and Von Dreele R B 2004 General structure analysis system (GSAS) *Los Alamos National Laboratory Report* LAUR 86–748

Megaw H D and Wells M 1958 The space group of $NaNbO_3$ and $(Na_{0.995}K_{0.005})NbO_3$ *Acta Crystallogr.* **11** 858–62

Miller S C and Love W F 1967 *Tables of Irreducible Representations of Space Groups and Co-representations of Magnetic Space Groups* (Pruett: Boulder)

Mishra S K, Ranjan R, Pandey D and Kennedy B J 2002 Powder neutron diffraction study of the antiferroelectric phase transition in $Sr_{0.75}Ca_{0.25}TiO_3$ *J. Appl. Phys.* **91** 4447–52

Mishra S K, Ranjan R, Pandey D and Stokes H T 2006 Resolving the controversies about the 'nearly cubic' and other phases of $Sr_{1-x}Ca_xTiO_3$ ($0 \leqslant x \leqslant 1$): I. Room temperature structures *J. Phys.: Condens. Matter* **18** 1885–98

Ranjan R, Pandey D and Lalla N P 2000 Novel features of $Sr_{1-x}Ca_xTiO_3$ phase diagram: evidence for competing antiferroelectric and ferroelectric interactions *Phys. Rev. Lett.* **84** 3726–9

Redfern S A T 1996 High-temperature structural phase transition in perovskite ($CaTiO_3$) *J. Phys.: Condens. Matter* **8** 8267–75

Rietveld H M 1969 A profile refinement method for nuclear and magnetic structures *J. Appl. Crystallogr.* **2** 65–71

Ringwood A E, Kesson S E, Reeve K D, Levins D M and Ramm E J 1988 Synroc *Radioactive Waste Forms for the Future* ed W Lutze and R C Ewing (Amsterdam: North Holland) pp 233–334

Sakowski-Cowley A C, Łukaszewicz K and Megaw H D 1969 The structure of sodium niobate at room temperature, and the problem of reliability in pseudosymmetric structures *Acta Crystallogr.* B **25** 851–65

Stokes H T, Hatch D M and Campbell B J 2007 *ISOTROPY* stokes.byu.edu/isotropy.html

Toby B H 2001 EXPGUI, a graphical user interface for GSAS *J. Appl. Crystallogr.* **34** 210–3

Xu H, Su Y, Balmer M L and Navrotsky A 2003 A new series of oxygen-deficient perovskites in the $NaTi_xNb_{1-x}O_{3-0.5x}$ system: synthesis, crystal chemistry and energetics *Chem. Mater.* **2003** 1872–8